Engineering Solid Mechanics 11 (2023) 191-204

Contents lists available at GrowingScience

Engineering Solid Mechanics

homepage: www.GrowingScience.com/esm

Design modification and performance evaluation of mini-hydrostatic pressure apparatus for inclined plane circular surface

Lawal Nasiru Muhammed[a], Ugheoke Benjamin Iyenagbe[a*] and Muhammed I. Wali[a]

[a]*Department of Mechanical Engineering, University of Abuja, Nigeria*

ARTICLE INFO

Article history:
Received 3 October 2022
Accepted 23 december 2022
Available online
23 December 2022

Keywords:
Hydrostatic test bench design, fluid systems
Hemispherical type design
Hydrostatic forces on inclined circular surface design
Covid-19

ABSTRACT

Mini-Hydrostatic Pressure Apparatus (MHSPA), of spatial size 230×210×210 mm^3, was developed for individual or limited number of users to promote Covid-19 social distance protocol. A solid hemisphere with an inclined circular segment made from gypsum material ($CaSO_2.0.5H_2O$) and coated with filler putty and oil paint, is used in place of the regular quadrants. With the solid attached to a horizontal beam mounted over a pivot, hydrostatic forces due to liquids were measured at different heights of water. The results showed that the assembly could be used to demonstrate variation of hydrostatic pressure on circular surfaces at different heights of liquid with an average difference of 4.38% against average theoretical values. Compared to other results from the use of conventional quadrants in literature, the associated error is minimal, and indicates the possibility of adopting the apparatus in school laboratories for static pressure demonstration.

1. Introduction

The effectiveness of experiments in understanding the scientific concepts of engineering sciences is an obvious fact (Basheer et al., 2016; Giridharan & Raju, 2016; Odom & Bell, 2015; Ching, 2014). The necessity for test equipment is supported by numerous reports, especially the neural underpinnings of vision presented by Ching (2014) and Kosslyn (1991), and the effect of laboratory environment on cognitive development reported by Niazi et al. (2018) and Davis et al. (2011). The learning pyramid created by the National Training Laboratories in Bethel as reported by Zhang (2020), stated that cognitive method of learning by doing (as commonly observed in laboratory experiments) increases the average retention rate from 5% to 90%. However, from the extracts of the report on equipment audit conducted by Committee on Needs Assessment of Nigerian Public Universities and cited by Ogunode and Adah (2022), revealed that physical facilities, especially laboratory equipment, for teaching and learning are inadequate, dilapidated, over-stretched/over-crowded and or obsolete. The growth in population in developing countries like Nigeria puts pressure on access to formal education. Thus, the country's universities and polytechnics need to acquire more laboratory equipment to cope with this increased demand for education access occasioned by population growth. Most equipment used for training are usually acquired from foreign countries, thereby putting pressure on and depleting the nation's foreign reserves. To minimize the negative consequences that equipment acquisition and maintenance have on the nation's foreign reserves, it is expedient to seek ways to leverage the benefits of the development of appropriate technologies using locally available materials with low capital and maintenance costs. The outbreak of the Covid-19 pandemic and the need to implement social distancing in laboratories further exposed the need for more basic training equipment and gave more credence to finding more ingenious ways to obviating the already exacerbated situation (Agusi et al., 2020). This formed the goal of the work reported in this paper, which is the design modification and performance evaluation of Mini-Hydrostatic Pressure Apparatus (MHSPA) intended for use as laboratory hydrostatic test

* Corresponding author.
E-mail addresses: ben.ugheoke@uniabuja.edu.ng (U. B. Iyenagbe)

ISSN 2291-8752 (Online) - ISSN 2291-8744 (Print)

doi: 10.5267/j.esm.2022.12.002

bench. The usefulness of a hydrostatic test bench cannot be overemphasized. Hydrostatic test benches are very useful in fluid systems design, installation, and maintenance. They help to understand force distribution features on fluid container walls. They are employed in diverse applications including marine floating and submerged systems, dams, canals, and culverts. It will be impossible for an engineer-in-training to have a rounded education given the dearth of basic training equipment such as hydrostatic test bench. Hydrostatic force (HSF) is the force of fluid at rest exerted on surfaces in contact with it (Nihous, (2016). Its magnitude varies directly as the depth of the fluid column. Such forces may grow up with height and exceed the resisting capacity of their containers and lead to system failure (Gulin et al., 2017; Agho et al., 2017). Thus, knowing the magnitude and characteristics of HSF is fundamental in the design, operation and maintenance of fluid storage and marine transport systems (FSTS) (Kim, 2011; Adesina, 2018). Hydrostatic force is also very useful in high pressure transmission equipment (Kumar & Prashanth, 2017; Iwan & Suyatna, 2018) and can be used to improve student's argumentation skills (G.U.N.T. Gerätebau GmbH, 2022; Ahmari & Kabir, (2019).

2. Materials and methods

2.1 Materials and equipment

The solid hemisphere is made from powdered Gypsum material, $CaSO_2.0.5H_2O$, due to its light weight (density of 2960 kg/m^3 at 20 ^{o}C), ability to spread and level evenly in molten state, and form hard surface to resist depression after drying. Fibre made from hardwood with a tensile strength of 135 MPa, and low density of 1,447 kg/m^3, is used as reinforcement (Patnaik, 2003; Kuqo & Mai, 2021; Jamala et al., 2013). Stainless Auto-K combination filler putty (Series (2021)) was used to seal the pores and smoothen the surfaces. An 18-litre high density polyethylene transparent container of dimension 350 mm × 210 mm × 210 mm, and thickness 1.5 mm, having a thermal rating of 65 ^{o}C, was adopted. An overhead beam made of mild steel of density of 7,800 kg/m^3 and modulus of elasticity of 220 MPa Engineering ToolBox (2004); Sultana, Hasan & Islam (2014, December)), caries cumulative loads to balance the HSF moments over a pivot. Other Accessories include a plastic scale to indicate liquid level, and bottom and side wooden frame to support the container. Predominantly, water is used for the tests due to its friendliness and free availability.

2.2 Features of Hydrostatic Pressure Apparatus

The most important features considered during the design synthesis of the hydrostatic test bench reported in this paper are as follows: The hydrostatic test bench consists of a transparent liquid container with drain valve to regulate liquid height. It is equipped with adjustable feet and spirit gauge to ensure balance of liquid surface. An overhanging beam, on which the quadrants, dead and balancing masses are hung, is placed on a pivot to provide free moment due to hydrostatic force. A level indicator with a thick mark corresponding to the position of equilibrium is located at one end. At the of the apparatus is the quadrant – with given surface configuration. A stainless-steel scale is attached to the side of the quadrant to indicate level of liquid in the container.

Two predominant hydrostatic bench designs currently used in most laboratories in Nigeria are typified by the plate shown in Fig. 1. The description of these predominant models of hydrostatic bench is adequately given in literature (Gerätebau GmbH, 2022, August 10; Ahmari & Kabir, 2019). The two models use the same principles of operation, and their operations and results are good. However, they are both used to measure hydrostatic forces on rectangular surface configuration only. Thus, hydrostatic test benches that can cater for vertical, and inclined circular surfaces for full and partial immersion are required to complement these existing designs. Such capability is considered in the current design reported in this paper.

Fig. 1. Existing Hydrostatic Pressure Apparatus

2.3 Review of Design Concept

The concept of hydrostatic force in liquids is based on Pascal's principle of pressure variation with depth. For a liquid of specific gravity $\gamma = \rho g$, and a column height z, at rest, the hydrostatic force exerted on the immersed surface of area is given as (Rajput, 2004):

$$F_h = \rho g z A \quad (1)$$

The principle of equilibrium of moments is used to balance the moment of the hydrostatic force, F_h, in Eq. (1) generated during immersion to attain stability. In the case of the hydrostatic apparatus, equilibrium is attained with the use of small masses, *m*, hung on the balancing arm as shown in Fig. 2.

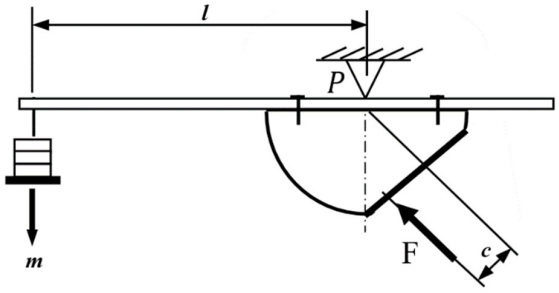

Fig. 2. Moment of the balancing weight about the pivot, P

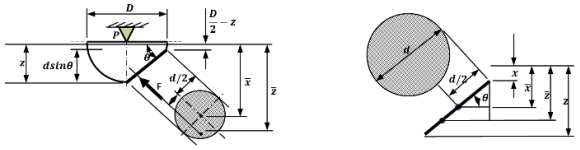

Fig. 3. Completely Immersed Inclined Circular Surface

With the configuration shown in Fig. 2, the statement of equilibrium is: $mg*l = F_h*c$. This provides means of obtaining the balancing mass, m from practical measurement as (Papaevangelou et al., 2006):

$$m = \frac{F_h \times c}{g \times l} \tag{2}$$

2.4 Design Assumptions

The basic requirements for the development of the MHSPA are:

i. Variation in pressure with depth of liquid must agree with Pascal's law (Jasim & Shamkhi (2020)).
ii. At full immersion, depth of water must < the radius of the solid hemisphere.
iii. Difference in the experimental values from theoretical ones should be < 15% (Helm).
iv. The container should be firm enough to prevent expansion due to the combined load it bears.
v. Local materials are used to minimize cost and improve availability of equipment.

To satisfy condition (i) all mechanical and hydraulic resistances to equilibrium systems are minimized.

To satisfy condition (ii), the diameter line BC = d, in Figure 2, is taken to be < D/2, where D is the diameter of the hemisphere.

To leave reasonable headroom for fully immersed condition, the vertical projection of OC is taken to be $\leq 0.042\ m$.

For the firmness of the container walls, the load of the overhead beam, water pressure on the container and containers weight were considered, at the bottom edge where the maximum impact tends to occur.

2.5 Geometric Model and Analysis of the Hemispherical Segment as an Immersed Body

The geometric model consists of a hemisphere of diameter D, with a circular segment of diameter, d, attached to an overhead balancing beam. The beam has two mass s, one on each end as dead and live weights. The vertical distance from the centroid of wetted area to the free surface $\bar{x}$, and the vertical distance from the of pressure to the free surface, $\bar{z}$, were determined in terms of the height of water z, the angle of inclination of circular plane, θ and the geometric properties of a circular segment.

Two models (configurations) were considered in this work: (a) fully immersed and (b) partially immersed inclined circular surfaces.

(a) Fully Immersed Inclined Circular Surface: The set-up for fully immersed circular surfaces is shown in Fig. 3.

The vertical distance from the free surface to the centroid of wetted area $\bar{x}$ is given as:

$$\bar{x} = z - \frac{d \times \sin\theta}{2} \tag{3}$$

where z is the depth of liquid from the free surface to the base of the hemisphere, d is the diameter of the circular segment and θ is the angle of inclination of the circular surface.
The vertical distance from the free surface to the of pressure is expressed as a function of the centroid of wetted area in Eq. (3) to give Eq. (4) as:

$$\bar{z} = \frac{(d \times sin\theta)^2}{16 \times \bar{x}} + \bar{x} \tag{4}$$

The turning moment due to the hydrostatic force, F_h in Eq. (1), on the inclined circular surface, OC, is shown in Fig. 4, with c, as the perpendicular distance of its line of action to the pivot, P.

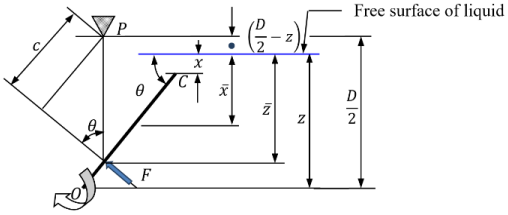

Fig. 4. Moment Effect of the HSF on inclined surface OC

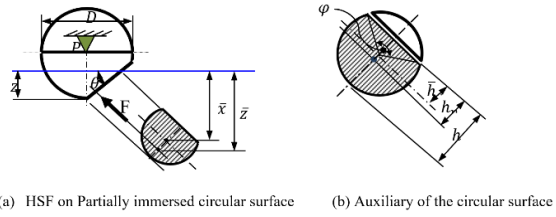

Fig. 5. Partially Immersed Inclined Circular Surface

The perpendicular distance, c, from the line of action of F to the pivot is given as a function the centre of pressure in Eq. (4) to Eq. (5) as:

$$c = \left[\left(\frac{D}{2} - z\right) + \bar{z}\right] \times sin\theta \tag{5}$$

(b) Partially Immersed Inclined Circular Surface: In this set-up, part of the circular surface area is above free surface of liquid level and the remaining segment is below it. The parameters of interest - height of water at any time, the centroid and of pressure of the wetted segment, designated respectively as z, $\bar{x}$, and $\bar{z}$ are shown in Fig. 5(a), with the blue line indicating the free surface of the liquid. Furthermore, two variables are added to the diameter, d of the circular surface: the subtended angle of the segment, φ, and the inclined height of the wetted segment h, as shown in the auxiliary view in Fig. 5(b).

The wetted segment area of the circular plane surface in terms of its wetted height, h, is given as:

$$A_p = \left[\frac{d^2}{4} cos^{-1}\left(1 - \frac{2h}{d}\right) - \left(\frac{d}{2} - h\right) * \sqrt{dh - h^2}\right] \tag{6}$$

where $h = \frac{z}{\sin\theta}$, is the height of the segment from the base, z is the vertical depth of liquid, and θ is the angle of inclination to the immersed circular surface to the free surface of water.

The vertical distance from the centroid of the wetted segment to the free surface is given as:

$$\bar{x} = \left[\frac{2d}{3} \times \left(\frac{\sin^3\frac{\varphi}{2}}{\varphi - \sin\varphi}\right) - \frac{d}{2} \times \cos\frac{\varphi}{2}\right] * \sin\theta \tag{7}$$

where the wetted surface segment subtended angle at the φ, is given as:

$$\varphi = 2 \times \cos^{-1}\left(1 - \frac{2z}{d \times \sin\theta}\right) \tag{8}$$

The distance of the of pressure from the free surface is given as:

$$\bar{z} = \frac{(I_{xx} - A_s\bar{h}^2) \times \sin^2\theta}{A_s \times \bar{x}} + \bar{x} \tag{9}$$

where I_{xx} is the moment of area of wetted segment about its diameter line, $\bar{h}$ is the distance from the centroid of the wetted segment to its diameter line, and A_s is the area of the wetted segment.

The distance from the free surface to the diameter line of the hemisphere is, $\frac{D}{2} - z$. Thus, the vertical distance of the of pressure to the pivot is:

$$\bar{z}_{cp} = \bar{z} + \left(\frac{D}{2} - z\right) \tag{10}$$

The mass required to balance the moment of the hydrostatic force, $F = \rho g A_c \bar{x}$, acting on a segment.

2.6 Design Analysis of the Model

The component sizes are based on their ability to bear both external live loads and inbuilt dead loads of the apparatus. The weight of each component of the system was determined as follows:

(a) The weight of the hemispherical segment:

This is obtained from:

$$w_h = 1.05 \times \frac{\pi g \rho_g}{3}\left[2\left(\frac{D}{2}\right)^3 - h_c^2 \times \left(\frac{3}{2}D - h_c\right)\right] \tag{11}$$

where ρ_g is the density of the gypsum material, g is acceleration due to gravity, D is the diameter of the hemisphere, and h_c is the cap height of the segment defined geometrically as:

$$h = \frac{1}{2}\left(D - \sqrt{D^2 - d^2}\right) \tag{12}$$

where d is the diameter of the cap segment and the coefficient 1.05 account for 5% by weight, of the fibre added to strengthen the hemisphere.

(b) Weight of the rod:

This is determined from:

$$w_r = 0.98 \times \rho_s g \times \frac{\pi d_r^2}{4} \times l_r \tag{13}$$

where d_r, is diameter of the rod and l_r, is its length. The factor 0.98 accounts for reduction in weight due to threaded part as well as anchorage holes and hanger slots.

(c) Dead weight balance:

The weight of the dead weight balance is obtained as follows:

$$w_d = \rho_s g \times \frac{\pi\left(D^2 - d^2\right)}{4} \times l \tag{14}$$

Weight of the transparent plastic container, w_c is calculated from:

$$w_c = [2h(L + B) + LB]t \times g \times \rho_p \tag{15}$$

where H is the height of the container, L is the length of the container, B is the breadth of the container, t_c is the thickness of the container, and ρ_p is the density of the plastic material.

(d) The weight of pivot assembly:

The weight of the pivot and accompanying lever is calculated from:

$$w_x = 1.025\ (BWt + 0.5Wht) \times \rho_s g \tag{16}$$

where b is the length of the pivot seat, e is the width of the pivot seat, t is the thickness of the plate, h is the height of the triangular pivot, ρ_s is the density of steel, and 1.025 is the joining factor for the weld joints.

(d) The maximum weight of liquid:

The maximum weight of liquid (water) the container can withstand is calculated from:

$$w_w = lbh \times \rho_w g \tag{17}$$

Total weight of the apparatus is obtained from the summation of all the weights as follows:

$$W_t = 1.25(w_h + w_r + w_d + w_c + w_x + w_w) \quad (18)$$

A weight factor of 25% was applied to obtain gross weight as indicated in Eq. (18).

(e) Sizing of the liquid container:

The size of the container is such that the immersion hemisphere can hang on the overhead beam freely without any obstruction by the sides and bottom of the container. A transparent plastic container having an approximate flat-end and a horizontal-elliptic cross-section shown in Fig.6, was used based on availability in market.

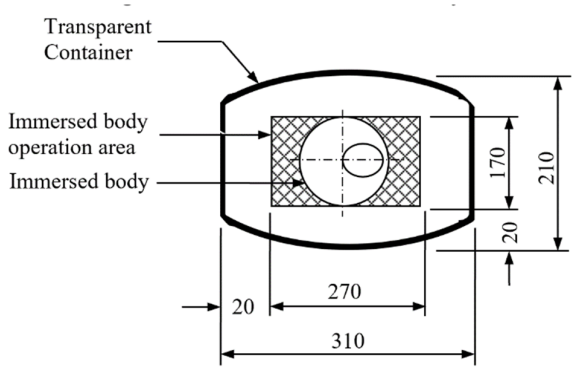

Fig. 6. Determination of the maximum allowable size of the quadrant

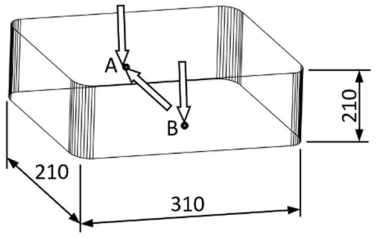

Fig. 7. Forces acting on the plastic container

The height of container is dependent on the radius D/2 of the hemisphere measured from its base. A 20 mm is given to provide underneath clearance from the base of the container as well as fixing of tap for emptying the container. Another 50 mm was given to damp out free surface wave due to outflow and inflow of water that could result to wrong reading of height of water. A head room of 50 mm was provided to contain overflow. Thus, the minimum height of the container is taken as D/2 +120 mm.

The geometrical dimension of the container was approximated to a cross sectional rectangle as shown in Fig. 8.

Two points - A and B are considered for adequate strength of the container.
For Point A: The hydrostatic force at the position of of pressure combined with other loads is given by:

$$W_h = \rho g A \times \bar{x} \quad (19)$$
$$W_v = k \times (W_t - w_w) \quad (20)$$

where *k* represents the percentage of the total vertical system load up to the point of pressure.
For Point B: The hydrostatic force at the base of the container combined with other loads is thus given in Eq. (21):

$$W_t = 1.25(w_h + w_r + w_d + w_c + w_x + w_w) \quad (21)$$
$$t = \frac{w_h}{l \times \sigma_p} \quad (22)$$
$$t = \frac{W_t}{2(l+b) \times \sigma_p} \quad (23)$$

2.7 System stability before immersion

The effective length of the beam was determined using the length of the container plus clearances to take care of the dead live balancing weights on each side of the beam shown in Fig. 8.

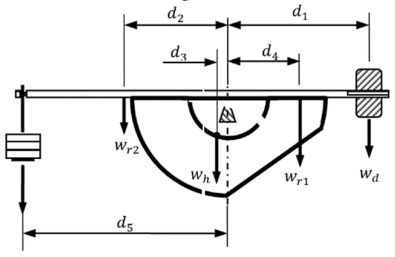

Fig. 8. Schematic assembled diagram of Overhead Beam

The beam is placed symmetrically on the container along its longitudinal length, L. A clearance of 75 mm is provided at each end of the beam, to provide space for the dead balancing weight on the right-hand side and for the small masses to be hung on the left-hand side, and another 15 mm to accommodate dangling of the hung loads. Thus, the total effective length is:

$$L_t = L + 2(L_c) + 15 \tag{24}$$

where L_t is the total effective length, L is the length of the container, and L_c is the clearance on each side of the beam.

(a) Dry balancing:

(i) The beam is loaded at four points as follows:
(ii) Dead weight, w_d, at a distance d_1 from the pivot
(iii) The weight of hemispherical segment m_h at a distance of d_3 from the pivot
(iv) Weight of the beam section to the left and to the right of the pivot, $w_r/2$, acting at distance of d_2 and d_4 respectively.

During dry balancing, weight of small masses is not used. Thus,

$$w_d \times d_1 + w_{r1} \times d_4 = w_h \times d_3 + w_{r2} \times d_2 \tag{25}$$

The diameter of the rod to withstand both deflection and moment is:

$$d = 2\sqrt{\frac{4w_r}{0.98 \times \pi\rho_s g \times l}} \tag{26}$$

3. Fabrication, assembly and testin

The construction of the MHSPA is divided into three main parts: the hemispherical segment, the overhead beam, and the container.

The hemispherical segment: A plastic ball of the same diameter as that of the hemisphere was obtained and divided into two equal parts, to produce the mould.

The trough of each side was identified as the base point of the circular segment to be removed. A pair of dividers was used to measure the required diameter of the segment and a second mark was produced at a distance d, from the first. The ball was then placed firmly on a vice with the two points vertically positioned (one above the other) and the segment cut off or milled off. The new circular opening was then covered from outside with a flat glass and adhesive tapes used to secure it in place. The description of the assembly is schematically and pictorially shown in Fig. 9 and Fig. 10 respectively.

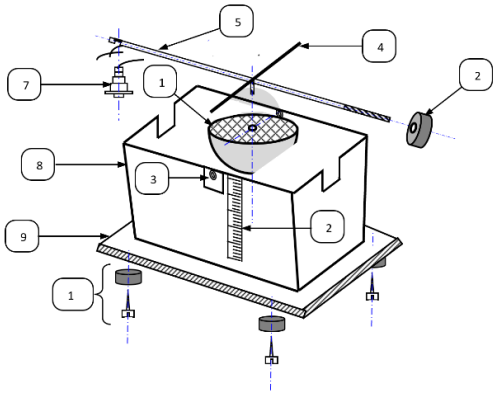

Fig. 9. Assembling process drawing of the MHSPA

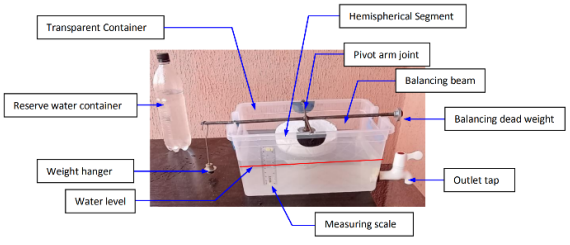

Fig. 10. Assembling process drawing of the MHSPA

The mould was placed upside down and a mixture of gypsum powder of ratio 2:1 was poured into it with a wooden fibre of about 2-5% of the total weight added to reinforce the block. The content was left for about 20 minutes and necessary adjustments done. The patter was left in the mould for about 6 hours to allow for adequate curing before the mould was removed. The final pattern obtained was again cured for 72 hours to allow for at least 75% of the water to be dried-off. It was next redressed before putty was applied to seal the pores to smoothen the flat surface. Red oxide paint was then applied twice as the final coating material.

Table 1. Part List for the Assembly

Part No.	Description	Material	Quantity
1	Hemispherical segment	Gypsum, putty and paint	2
2	Balancing dead weight	Mild steel	1
3	Pivot beam anchorage	Force fit bearings	2
4	Pivot beam	Mild steel circular rod	1
5	Balancing beam	Mild steel circular rod	1
6	Balancing live weight	Cast Iron (In various sizes)	5 – 350 g
7	Plastic container	Plastic (transparent)	1
8	Container base wooden rest	Plywood (3/4'')	1

The overhead beam (5), is made from a mild steel rod of diameter 8 mm, and a length 0f 355 mm. A thread of size 10 mm and a pitch 1.5 is cut on one end for a length of 100 mm using a die-set for external threading. On the other side a groove of width 3 mm and depth 2 mm was produced to hold the hanger (7) in place. A hole of diameter 3 mm was bored through laterally at the of the rod and a 3 mm rod was forced fitted into it and extended outwards to each side of the hole by a length of 110 mm. A rod of 4 mm was used to form the pivot seat (4) with its ends embedded in a hole at each lateral side of the container. In this hole is placed a bearing-like hollow and this cylinder for easy rotation of the pivot rod. The dead weight (2) was produced from a mild steal blank of diameter 80 mm and length 60 mm. An M10 internal thread was cut through its across its length to match the external thread produced on the overhead beam. A transparent plastic container (8) of about the required size was adopted and necessary adjustments were made to accommodate all the mating parts.

The schematic diagram of the assembly is presented in Figure 11 with a parts list containing description of the components, quantity required and the materials from which they are made.

3.1 Structural and Operational Tests

The tests conducted were categorized into two, viz:

(a) Structural tests, which were meant to determine the impact of water and extreme temperature on the apparatus. These include rupture test, and liquid temperature test.

(b) Operational tests, designed to determine maximum displacement and variation of pressure with depth. These include maximum displacement angle and linearity tests.

3.2 Rupture Tests

The hemispherical segment was placed in water for a continuous period of 72 hours. The initial weight of the disc was measure and recorded. After every 6 hours, the disc was removed, cleaned, and measured again. The experiment was repeated for three days. In each case, the weight and time that elapsed while disc was soaked in water were recorded. The quantities of water sucked by the disc were determined by differences in successive weights to evaluate the rupture tendency of the block.

3.3 Liquid Temperature Test

Temperature test was used to estimate the impact of variation in hydrostatic force with environmental and liquid temperature which could result to thermal expansion capable of causing variation in measured height of water (Saehana, Ali & Supriyatman (2019)). At the start of experiment, water at room temperature of 27 ^{o}C was used. The temperature was then increased at interval of 5^{o} until 55 ^{o}C was reached. Each time, the level of water in the container was noted and the average variation in hydrostatic forces determined.

3.4 Maximum Displacement Angle

This test was conducted to determine the maximum level of free surface required during full immersion for the experimental results to remain reliable.

All the forces, F_1 through F_4 on the circumference pass through the pivot point, P and thus, have zero turning moment effects. The moment due to resultant hydrostatic force, F_R will be amplified by the presence of F_d, due to water getting to the top flat face of the hemisphere. This will result to amplification of F_R and thus, affecting the accuracy of the results. To avoid this, the tip of the flat surface must not be allowed to tilt below the free surface. In this case, F_R was gradually increased by increasing the water level, and the angular displacement of the hemisphere in each case was noted.

3.5 Linearity Test

The resultant hydrostatic force on immersed surface is based on Pascal's principle which states that pressure increases with depth. Thus, $p = kh$, where $k = \rho g$. To test for the operation of the apparatus to meet this definition, water level was

gradually increased and the small masses used to counter the hydrostatic force generated. The results were used to determine the type of relationship between the two variables.

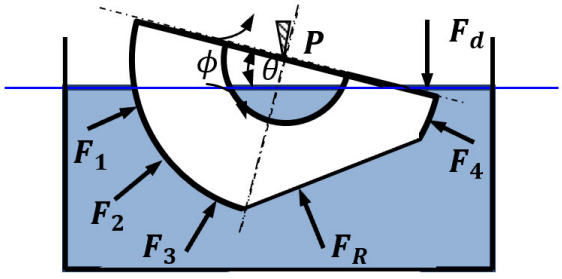

Fig. 11. Maximum displacement of the semi-circular disc for accuracy

3.6 Test Procedures

The procedure used was based on Ahmar and Kabir's Applied Fluid Mechanics Lab Manual (Ahmari & Kabir (2019)) and the setup of (Jazaei (2020)). The radial dimensions of the hemisphere and the circular segment, the distance of the small balancing loads and dead load distances to the pivot were first measured and noted. Dry balancing was then conducted by turning the dead weight along the screw thread to set the beam on horizontal equilibrium against the weight of the hemisphere. This was followed with a known quantity of weights (in grams) placed on the weight hanger to dis-balance the beam. Next, water was gradually added to the container until it enough hydrostatic force was generated to balance the beam back to horizontal position. The levels of water in the container at each point of equilibrium were recorded. Finally, the balancing weights were gradually reduced in turn, to the dis-place the beam once again while more water was also drained out each time to again balance the beam. In all cases the average value of the hydrostatic force required to balance set quantity of weight with the corresponding pressure were determined.

4. Results and discussion

The results presented cover the development of a mini-hydrostatic pressure apparatus with mathematical analysis and simulations for fully and partially immersed inclined circular plane surfaces. A practical demonstration to validate its structural and operational fitness to use was conducted.

4.1 Basic Final Design Dimensions

The basic dimensions of the parts of the prototype developed are presented in Table 4, using Equations (11) through (25), based on structural and operational requirements of the apparatus.
The maximun internal dimension of the container is 315 × 205 × 120 mm^3. The external spatial dimension is 457 × 230×250 mm^3 with an approximate gross weight of 7.5 kg. The immersed hemispherical segment has a diameter of 157 mm and circular segment of 82 mm. The maximum rated load for the balancing beam is 1.025 kg with a working balancing load of 420 g.

The height of container is dependent on the radius, D/2 of the hemisphere measured from its base. A 20 mm gap is given to provide underneath clearance from the base of the container as well as fixing of tap for emptying the container, as shown in Fig. 7. Another 50 mm is given at the top to damp out free surface wave due to outflow and inflow of water that could result to wrong reading of height of water. A head room of 50 mm was provided to contain overflow. Thus, the minimum height of the container is taken as D/2 +120 mm.

Table 2. Critical dimension of the major component parts

S/N	Description	Design Size	Unit
1	Liquid container internal dimension	315 × 205 × 120	m^3
2	Hemispherical Segment Diameter	157	mm
3	Circular segment diameter	84	mm
4	Hemisphere Anchorage Screw	M11	mm
5	Balancing Beam Diameter	8	mm
6	Pivot seat cross-rod diameter	4	mm
7	Distance from balancing weight to the pivot (RS)	235	mm
8	Distance from dead weight to the pivot (CS)	200	mm
9	Maximum balancing load	420	g
10	Maximum rated load on the beam	1,025	g

4.2 Water Penetration and Rupture of the Hemispherical Segment

Before placing the hemisphere in water, its weight was measured using a digital balance. After the specified interval of time, it was measured again as indicated in Section 3.1. The consecutive differences in weight are the details shown on the vertical axis of Fig. 12 measured over 72 hours. As seen from Fig. 12, three phases are distinguishable in the rate at which water penetrates the coating materials or overcome the resistance offered by the coating materials, in turns from outside inwards. These segmente represent the resistances from the red oxide paint, the filler putty and Gypsum poor phases.

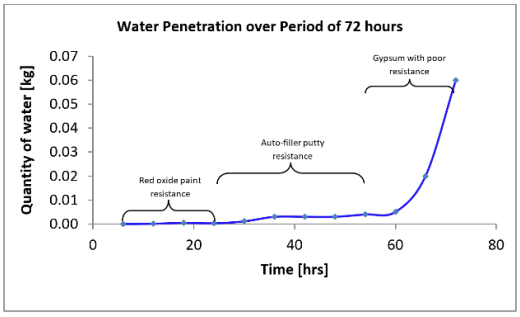

Fig. 12. Rupture Test Results

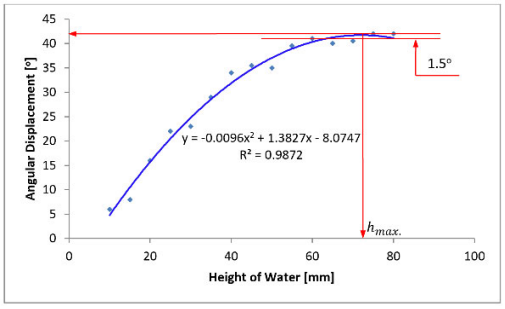

Fig. 13. Maximum water height for stability

For the first 25 hours in water the hemispherical block offered a very high resistance to water absorption due to the application of red oxide paint as the external coating. As such, the rate of water absorption is almost zero. The segment in the graph (Fig. 12) is indicated as red oxide paint resistance. After 25 hours, there was a gradual increase in the rate of water absorption but tends to remain constant from 35th hour to about the 55th hour. During this interval, an average water absorption rate of 4g was maintained due to intermediate resistance offered by the auto-putty filler. Beyond this period, the gypsum got exposed to water and the rate of absorption surged exponentially from 10 g on the 60th hour to 72 g at the 70th hour, giving an average rate of 6.2 g/hr. The apparatus is scheduled to operate on a maximum of 8 hours per day after which the block will be taken out cleaned and aired for proper drying and storage, as against 25 hours period during which it can lose its external protections. With this condition, the putty and paint protection are very adequate.

4.3 Angular displacement of the hemisphere

The angular displacement of the hemisphere against height of water for combined partial and full immersions is displayed in Fig. 14. The range of the height of water covered is between 10 to 80 mm. The general feature of the relationship between height of water and angular displacement of the hemisphere block is quadratic, for the combined range. At water height, z = 10 mm, the hemisphere was displaced 6^{o}. This displacement increases almost linearly up to a water height of z = 40 mm where its value is 34^{o}, representing on average 0.72^{o} per rise in water height. Beyond that range, the graph tends to be quadratic and gradually and attained maximum displacemet of 42^{o} at a water height of 72 mm. Thus, based on design requirement of 0.1294D in Section (2.4) - item ii, with a hemisphere diameter of 157 mm, the highest water level is less than D/2 (78.5 mm). For reliable results, a headroom of at least 7% representing 4 mm, is provided. This leaves the possible maximum height of water available to be 74.5 mm. (40 mm for partial imerssion and 35.5 mm for full immersion). With an allowance of 4 mm left to prevent water from getting to the top flat surface of the hemisphere, the maximum angular disphencement is less than 42^{o} by about 1.5^{o}, as shown in the graph of Fig. 13, which satisfies the design.

From the graph (Fig. 13), the rate of angular displacement for fully immersed region (40 mm – 75.5 mm) is 0.21^{o} per mm on average, thus for a headroom of 4 mm, the equivalent angular displacement is 0.82^{o}. This value is less than the 1.5^{o}, which is the maximum allowable tilt angle the hydrostatic test bench is designed to accommodate.

4.4 Impact of temperature on height of Water

Fig. 12 gives the variation of the height of water with temperature using the container only without the hemisphere. The condition investigated with reference to Nigeria climate has a wide range of temperature from about 20 ^{o}C in the southern part to about over 40 ^{o}C in the far North.

As the water in the container is gradually heated as discussed in Section 3.2, the height of water level drops with approximately two sections, A and B indicated in Fig. 14, with slopes of the sections representing rates of change in height per unit increase in temperature. In section A, the height of water initially remains constant at about 118.5 mm increase in water temperature from 10 ^{o}C to 20 ^{o}C. Further increase in temperature causes slight drop in water height by about 0.25 mm with a rate of 0.008 mm/^{o}C. Beyond this temperature is a sharp reduction of about 1.5 mm over 15^{o} rise in temperature giving a reduction rate of 0.1 mm/^{o}C. All these reductions are due to expansion of the container as the temperature increases. With volume remaining approximately constant, increase in cross sectional area results to reduction in height. The overall average

height variation of 2.1 mm is very small compared to the maximum attainable height of 74.5 mm. This height variation is approximately representing possible error of 2.8%.

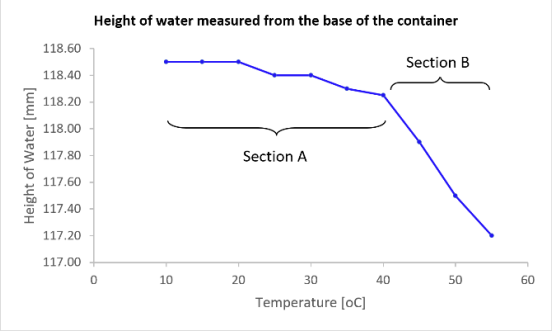

Fig. 14. Variation of height of water with incraese in temperature

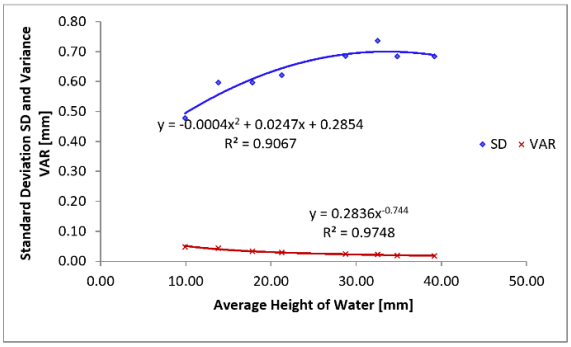

Fig. 15. Maximum error involved with the use of the apparatus

4.5 Standard Deviation and Variance of Errors due to Measurements

Fig. 15 presents the possible magnitude of error due to several factors that could cause inaccurate results. The spread of this error over a range of approximately 10 mm to 40 mm height of water are indicated with the standard deviation and variance from results population of 15 runs of experiments.

The best fit for standard deviation (SD) is quadratic function ($y = -0.000x^2 + 0.024x + 0.285$) while that of variance is a power function ($y = 0.283x^{-0.74}$) as shown in the graph of Fig. 15. For the standard deviation, it increases from 0.48 mm at 10 mm height of water to an average maximum of 0.7 mm at approximately 40 mm of water height. The maximum variance is 0.05 mm at 10 mm and reduces to 0.02 mm at about 32 mm of water height and thereafter remained steady at that value even as the height of water increases to approximately 40 mm. The corresponding R^2 values for SD and VAR are respectively 0.91 and 0.98. This is an indication that the error distribution is adequately and randomly represented by the given function as between 91% and 98% of the data points were utilized to fit the SD and VAR curves respectively. This result agrees with the findings of Helm in which the maximum SD of 8 mm was reported over a water height range of 120 mm representing an error of 6.67%. It also falls below the 3.26% average error reported in the statistical analysis of experimental hydrostatic forces against simulated values by Papaevangelou et al. (2006).

4.6 Operational suitability

The results obtained in demonstrating the operation of the MHSPA to validate the mathematical relation provided in Eq. (1) through (10) are presented in Fig. 16 through Eq. (18). They basically show the variation of pressure with depth of water, vertical variation in of pressure and centroid of area using equations generated and experimental values.

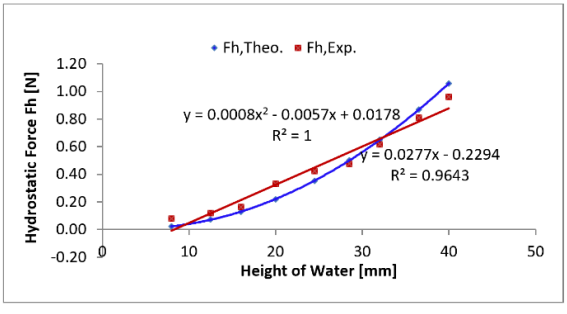

Fig. 16. Variation of Hydrostatic force against Height of Water

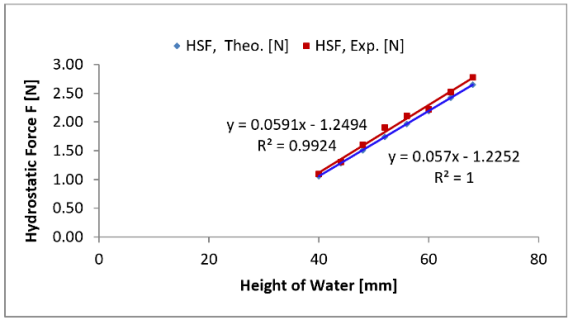

Fig. 17. Experimental and Theoretical Hydrostatic forces

Fig. 16 presents the graph of hydrostatic force against water height in the container for partially immersed circular surface. Theoretically, the graph is quadratic as predicted by the related formula in (1) and (6) but tends to be more linear in the experimental result. In both cases, hydrostatic pressure increases with increase in height of water, this is significant as it agrees with the Pascal's principle. The increase in the theoretical force is slower at the beginning and becomes more rapid after half of the circular shape was immersed. This profile is also supported by the projected area of the inclined circle on a vertical plane, which will turn out to be elliptical. With the edge smaller than the centre area, hence the applied hydrostatic forces on

the edges grow gradually and fastened up towards its centre. The experimental force in red colour intercepts the vertical line at the negative side of the graph (-0.227 N). This is as a result of possible frictional force and other resistances opposing its take-off until at an average water height of 7.5 mm. Thereafter, it increases at a rate of 0.027 N/mm of water rise. The theoretical graph in blue has all its points aligned to give an R^2 factor of 1, where the Experimental value gives an R^2 of 0.96. This indicates a difference of about 4% difference between the two sets of data points.

Fig. 17 is the hydrostatic force on fully immersed inclined circular surface. Both theoretical and practical forces are linear with an average difference of 0.09 N across the range of water height. Again, both theoretical and experimental data points show increase of pressure with depth of water (Pascal's principle). In fully immersed scenario however, the theoretical graph is linear, showing that as depth of water increases, the influence of area diminishes. Secondly, the two lines are almost parallel with a slope difference of 0.021 N/mm. In both cases on average, the experimental hydrostatic force is slightly higher than the theoretical values. This is expected as some mechanical resistance and fluid viscosity in the experimental situation and not accounted for in the theory. This difference is however very low here as indicated in their R^2 of 0.0076.

The set of points are more streamlined than in the partial immersion scenarios. They both have an intercept at about -1.2 N and increase steadily at an approximate rate of 0.06 N/mm.

Fig. 18 presents the variation of centres of pressure and immersed area against depth of water using Eq. (3) and Eq. (4) for partially immersed and Eq. (7) and Eq. (9) for fully immersed conditions. Both scenarios are shown on one graph with demarcation at 40 mm water height.

In this work, the depth of water to the centre of area and pressure are measured from the free surface of water. Thus, the graph the centre of pressure in red is always at a higher depth than that of the centre of area. This description agrees with the theoretical relations given in Eq. (9) for centre of pressure has two positive terms, one of which is Eq. (7) for centroid, which shows that the value from Eq. (9) is greater than that from Eq. (9). That is the distance of centre of pressure from the surface is always below that of centroid from the free surface. $Cp = k + Cg$. Where k is a factor influenced by the magnitude of the moment of immersed area.

Also, the gap between the two centres increases from low water level at 10 mm to its maximum at just fully immersed and then, gradually reduces back again as in Fig. 18. This suggests that when the area immersed is small, the centroid and centre of pressure are very close and becomes farther away as the more area is immersed. Further away beyond the region of partially immersed, the gap between the two graphs closes again. This shows that when an object is shallowly immersed or deeply immersed in water, the line of action of the resultant hydrostatic force tends to pass through its centre of gravity. This is a very useful indication as large differences between centroid and centre of pressure could result to imbalance in centrifugal force and hydrostatic forces on rotating member at such depth.

5. Conclsuion

A mini-hydrostatic pressure apparatus for demonstrating the Pascals principle of pressure increase with depth of liquid was developed with a compact size of 315 × 205 × 120 mm^3 and a total weight of 7.5. The components were built using locally available materials. The model was tested via six sets of experiments: three for partially immersed and three for fully immersed scenarios, to evaluate variation of hydrostatic pressure and of pressure with depth of water on immersed inclined circular plane surface. The results obtained show significant success as the percentage difference between the theoretical values and experimental ones are below 5% in all cases, and they are also in agreement with the reports of Jasim and Shamkhi (2020) and Helm.

The MHSPA can be perfected and developed for use in school laboratories and commercial purpose. Finally, Pascal's theory of pressure increase with depth and variation of s of area and pressure are achieved with the apparatus. The apparatus could therefore be used in laboratories. The design approach and framework could be helpful to developing nations having difficulties with foreign reserves and cashflows.

Acknowledgement

The researchers are greatly indebted to Engr. Saad AbdulRazaaq, for his time and contribution to the construction of the apparatus.

References

Adesina, F. (2018). Design and fabrication of a manually operated hydraulic press. *Open Access Library Journal*, *5*(04), 1.

Agho, N., Mailabari, S. K., Omorodion, I. H., Ariavie, G. O., & Sadjere, G. E. (2017). Design Construction and Testing of a Petroleum Product Storage Tank 10 Million Litre Capacity. *European Journal of Engineering and Technology Research*, *2*(3), 48-52.

Agusi, E. R., Ijoma, S. I., Nnochin, C. S., Njoku-Achu, N. O., Nwosuh, C. I., & Meseko, C. A. (2020). The COVID-19 pandemic and social distancing in Nigeria: ignorance or defiance. *The Pan African Medical Journal*, *35*(Suppl 2).

Ahmari, H., & Kabir, S. M. I. (2019). *Applied Fluid Mechanics Lab Manual*. Mavs Open Press.

Basheer, A., Hugerat, M., Kortam, N., & Hofstein, A. (2016). The effectiveness of teachers' use of demonstrations for enhancing students' understanding of and attitudes to learning the oxidation-reduction concept. *Eurasia Journal of Mathematics, Science and Technology Education*, *13*(3), 555-570.

Ching, C. P. (2014). Linking theory to practice: A case-based approach in teacher education. *Procedia-Social and Behavioral Sciences*, *123*, 280-288.

Davis, F. J., Lockwood-Cooke, P., & Hunt, E. M. (2011). Hydrostatic pressure project: Linked-class problem-based learning in engineering. *American Journal of Engineering Education (AJEE)*, *2*(1), 43-50.

Engineering ToolBox, (2004). Metals and Alloys - Densities. [online] Available at: https://www.engineeringtoolbox.com/metal-alloys-densities-d_50.html. Retrieved December 23, 2022, from https://www.engineeringtoolbox.com/metal-alloys-densities-d_50.html

G.U.N.T. Gerätebau GmbH (2022, August 10). Experiment for Engineering Education, Instruction Manual HM 150.05 Hydrostatic Pressure Apparatus, Pp 1-19, 2022. Retrieved December 23, 2022, from http://www.gunt.de/en/products/hydraulics-for-civil-engineering/fundamentals-of-fluid-mechanics/hydrostatics/hydrostatic-pressure-in-liquids/070.15005/hm150-05/glct-1:pa-148:ca-173:pr-552?googleTranslate=1

Giridharan, K., & Raju, R. (2016). Impact of teaching strategies: demonstration and lecture strategies and impact of teacher effect on academic achievement in engineering education. *International Journal of Educational Sciences*, *14*(3), 174-186.

Gulin, M., Uzelac, I., Dolejš, J., & Boko, I. (2017). Design of Liquid-Storage Tank: Results of Software Modeling Vs Calculations According to Eurocode. *Advances in Civil and Architectural Engineering*, *8*(15), 85-97.

Helm, R. Hydrostatic Pressure on a Partially and Fully Submerged Vertical Rectangular Surface.

Iwan, M., & Suyatna, A. (2018). Development of Static Fluid Learning Props to Improve Students' Argumentation Skills. *International Journal of Research Granthaalayah*, *6*(6), 296-309.

Jamala, G. Y., Olubunmi, S. O., Mada, D. A., & Abraham, P. (2013). Physical and mechanical properties of selected wood species in tropical rainforest ecosystem, Ondo State, Nigeria. *IOSR Journal of Agriculture and Veterinary Science (IOSR-JAVS). eISSN*, 2319-2380.

Jasim, N. A., & Shamkhi, M. S. (2020). The design of the center of pressure apparatus with demonstration. *Cogent Engineering*, *7*(1), 1843225.

Jordaan, J. M., & Bell, A. (Eds.). (2009). *Hydraulic Structure, Equipment and Water Data Acquisition Systems*. Eolss Publishers Company Limited.

Kim, S. P. (2011). CFD as a seakeeping tool for ship design. *International Journal of Naval Architecture and Ocean Engineering*, *3*(1), 65-71.

Kosslyn, S. M. (1991). A cognitive neuroscience of visual cognition: Further developments. In *Advances in psychology* (Vol. 80, pp. 351-381). North-Holland.

Kudela, H. Hydrostatic Force on a Plane Surface.

Kumar, S., & Prashanth, B. (2017). Design and fabrication of hydraulic press. *Int. J. Sci. Develop. Res*, *2*(7), 227-230.

Kuqo, A., & Mai, C. (2021). Mechanical properties of lightweight gypsum composites comprised of seagrass Posidonia oceanica and pine (Pinus sylvestris) wood fibers. *Construction and Building Materials*, *282*, 122714.

Niazi, M. U. R. K., Asghar, M. A., & Ali, R. (2018). Effect of Science Laboratory Environment on Cognitive Development of Students. *Pakistan Journal of Distance and Online Learning*, *4*(1), 123-134.

Nihous, G. C. (2016). Notes on hydrostatic pressure. *Journal of Ocean Engineering and Marine Energy*, *2*(1), 105-109.

Odom, A. L., & Bell, C. V. (2015). Associations of Middle School Student Science Achievement and Attitudes about Science with Student-Reported Frequency of Teacher Lecture Demonstrations and Student-Centered Learning. *International Journal of Environmental and Science Education*, *10*(1), 87-97.

Ogunode, N. J., & Adah, S. (2022). Accreditation of Academic Programs in Public Universities in Nigeria: Challenges and Way Forward. Electronic Research Journal of Social Sciences and Humanities, 4(2), 15-27.

Papaevangelou, G., PSILOVIKOS, A., & IOANNIDIS, D. (2006). Statistical analysis and simulation of a hydrostatic force experimental device. In *Proceedings of the 2006 IASME/WSEAS Int. Conf. on Water Resources, Hydraulics & Hydrology* (No. IKEECONF-2018-052, pp. 81-85). Aristotle University of Thessaloniki.

Patnaik, P. (2003). *Handbook of inorganic chemicals* (Vol. 529, pp. 769-771). New York: McGraw-Hill.

Rajput, R. K. (2004). *A textbook of fluid mechanics and hydraulic machines*. S. Chand Publishing.

Saehana, S., Ali, M., & Supriyatman, S. (2019). Thermal Expansion and Hydrostatic Pressure Experiment Using Common Materials for Supporting Science Education in a Rural Area at Central Sulawesi, Indonesia. *Jurnal Pendidikan IPA Indonesia*, *8*(2), 241-246.

Series, T. (2021). Product data sheet. *SimulateIR-D-01-A Model*, *5236*.

Sultana, M. N., Hasan, M. F., & Islam, M. (2014, December). Analysis of Mechanical Properties of Mild Steel Applying Various Heat Treatment. In *Proceedings of the International Conference on Mechanical, Industrial and Energy Engineering, Khulna, Bangladesh* (pp. 25-26).

Zhang, J. (2020, August 23). *Learning Pyramid: A Way To Learn Knowledge*. Medium. Retrieved December 23, 2022, from https://saneryee-studio.medium.com/learning-pyramid-a-way-to-learn-knowledge-ac295e2e1395